Optical Coherence Correlation Spectroscopy on Gold Nanoparticles for Point-of-Care Immunoassays

Daniel Migliozzi

Semester Project Report, January 2014

Master: Bioengineering

Minor: Biomedical Technologies

Project Director: Theo LASSER

Supervisors: Stéphane BROILLET, Ivan MAERKI

Laboratory: Laboratoire d'Optique Biomédicale (LOB), Ecole Polytechnique Fédérale de Lausanne (EPFL)

Abstract

The interest in very sensitive diagnostic techniques pushes towards the development of always new detection methods. Here we present a technique to perform immunoassays based on the detection of gold nanoparticles (NPs) via analysis of their scattered light. This interferometric method, called Optical Coherence Correlation Spectroscopy (OCCS), allows both the analysis of several sampling volumes simultaneously, such as Optical Coherence Tomography (OCT), and correlation measurements similar to Fluorescence Correlation Spectroscopy (FCS). The aim of this project was to give a proof of concept of OCCS to perform immunoassays: this technique was used to measure several values of the diffusion coefficient of gold NPs in the presence of different concentrations of either specific or non-specific antibodies. We studied immunoassays with OCCS in solution in well-plates, and verified the coherence of some results with FCS. We worked with streptavidin-coated gold NPs in the presence of anti-streptavidin or anti-β-lactoglobulin. We found that the coating does not affect the diffusion of the NPs with respect to their naked form. Conversely, the presence of anti-streptavidin in solution has major consequences on their motion. A small interaction is suspected to exist between coated-NPs and the non-specific antibody, but statistical analysis seems to infirm this fact. Still, a putative non-specific interaction has been found between non-coated NPs and anti-streptavidin, which could result from adsorption of the body of the antibody onto the NP surface. Optimization of the size and the concentration of the gold NPs for OCCS measurements could result in a sensitive manner to detect antibodies in in blood sample (e.g. to diagnose allergies). Furthermore, as in OCCS the sampling volume is no more limited to a small confocal volume, novel solutions for sensing in microfluidic channels would be interesting to investigate.

Contents

1 Optical methods for immunoassays **4**

2 The theoretical and experimental tools **5**
2.1 Optical Coherence Correlation Spectroscopy 5
2.2 The experimental setup 7

3 Results **9**
3.1 Theoretical probing of the coating 9
3.2 Study of gold NPs with xf-OCM 10
3.3 FCS on gold NPs 11
3.4 OCCS on gold NPs 14
3.5 Discussion 17

4 Conclusion **20**

A Modelling of NP diffusion **22**

B FCS additional graphs **24**

Chapter 1

Optical methods for immunoassays

The problem of molecules detection for point-of-care diagnostics is a topic on which many research groups in the field of lab-on-chip work, as well as many companies in the pharma or biomedical sector[1, 2]. The possibility to measure infinitesimal quantities of a bio-molecule in a sample creates a powerful improvement in clinical diagnostics as well as in drug discovery. In many cases, what is studied by the device is the interaction between the target molecule and the probes one uses for the capture. This should be a specific interaction which allows to restrict the detection to the analytes of interest, from which the capability to reach such high sensitivities. Several are the methods implemented for the detection, they utilize electrical[3], biochemical[4] and optical[5] phenomena.

In optics, many advancements have been done to perform point-of-care studies[6]. A promising tool is based on the self-interference of low-coherence light. Letting a more detailed inspection of what this phenomenon is to the section 2.1, Optical Coherence Correlation Spectroscopy (OCCS) is based on the well known Optical Coherence Microscopy (OCM)[7]. This is a powerful means for measuring back-scattered light from objects to be detected. As a plus, it allows the localization of the target object not only on the lateral axis but also along the longitudinal axis with only one measurement, which is very difficult with other optical techniques such as fluorescence microscopy (FM) and even impossible with non-optical methods, which can only give information about the amount of the target in the sample. Moreover, with respect to FM, OCCS does not suffer from photobleaching and other major problems of fluorescent molecules. As scattering objects, gold nanoparticles (NPs) are very good candidates, because they are almost inert in biological media, are available with several kinds of coating (e.g. antibodies) and their metallic nature gives the possibility to exploit other useful phenomena such as plasmonic resonance[8] or photothermal effect[9]. The absence of biochemical reporters (like enzymes as in ELISA for example) is also a further advantage towards the stability and the durability of the method.

In the Laboratory of Biomedical Optics (LOB), it has already been shown that it is possible to measure the size and the concentration of gold nanoparticles in wells by using OCCS[9, 10]. The aim of this project was to verify the possibility to perform an immunoassay with OCCS by using gold nanoparticles.

Chapter 2

The theoretical and experimental tools

2.1 Optical Coherence Correlation Spectroscopy

Optical Coherence Correlation Spectroscopy (OCCS) is a technique based on Optical Coherence Microscopy (OCM), with some further advantages from correlation analysis. For a detailed treatment of OCM one can refer to [7, 13]. Here we only report some basic concepts on this method.

OCM uses the wave nature of light to get information about the sample: by analyzing the back-scattered light from an illuminated object, one can obtain a 3-dimensional view of it. The principle is the following. An interferometer (fig. 2.1) is used to make the back-scattered light interfere with a reference

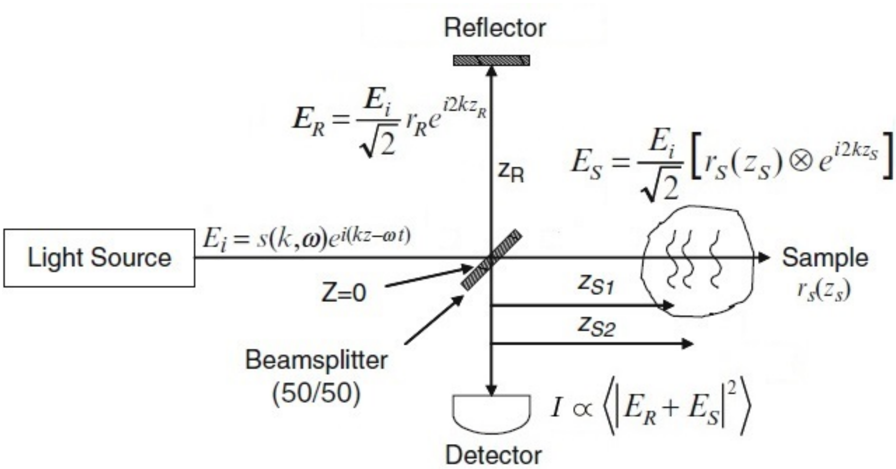

Figure 2.1: **Interferometer as used in OCM.** The notation for the electric field in the different regions of the interferometer. Adapted from [7]).

beam. The resulting spectrum is then analyzed to obtain information on the position of the object along the longitudinal axis. The interferometer is illuminated by polychromatic light, the electric field of which can be expressed as $E_i = s\left(k,\omega\right) e^{i(kz-\omega t)}$, where $s\left(k,\omega\right)$ is the electric field amplitude as a function of the wavenumber and the angular frequency of the incoming light. The beam-splitter is supposed to have an achromatic power splitting ratio of 0.5 and is taken as the origin for all the distances calculated (e.g. z_R is the distance of the beam-splitter from the refencence reflector, and z_{S_n} is its distance from each reflector inside the sample). The reflection coefficients of the reference reflector and the sample are respectively defined as r_R and $r_S\left(z_s\right) = \sum_n r_{S_n} \delta\left(z_S - z_{S_n}\right)$, where the sum of delta distributions indicates the dependence of the reflection coefficient on the depth of the reflective object, here supposed to be composed of discrete reflector planes. With this notation, the fields on the beam-splitter after returning from the reference and sample arms are given by $E_R = \frac{E_i}{\sqrt{2}} r_R e^{i2kz_R}$ and $E_S = \frac{E_i}{\sqrt{2}} \sum_n r_{S_n} e^{i2kz_{S_n}}$ respectively.

Thus, the intensity reaching the photo-detector is given by these two interfering fields $I \propto \left\langle \left| E_R + E_S \right|^2 \right\rangle$

and reads

$$I(k) \propto S(k)\left[\underbrace{R_R + \sum_n R_{S_n}}_{\text{DC Term}} + \underbrace{\sum_n \sqrt{R_R R_{S_n}}\cos\left[2k\left(z_R - z_{S_n}\right)\right]}_{\text{Cross-correlation Term}} + \underbrace{\sum_{m\neq n} \sqrt{R_{S_m} R_{S_n}}\cos\left[2k\left(z_{S_m} - z_{S_n}\right)\right]}_{\text{Auto-correlation Term}}\right] \tag{2.1}$$

where $R_l = |r_l|^2$ are the reflectivities, and $S(k) = \left\langle |s(k,\omega)|^2 \right\rangle = \frac{1}{\Delta k\sqrt{\pi}} e^{-\frac{(k-k_0)^2}{\Delta k^2}}$ is the power spectrum of the illumination light, k_0 being its central wavelength and Δk its spectral bandwith.

The "DC term" is a pathlength-independent offset which is close to R_R, because of the much larger reference reflectivity compared with the sample reflectivity. The "Cross-correlation term" is the desired information about the sample (i.e. $\sqrt{R_S(z_s)} = \sum_n \sqrt{R_{S_n}}\delta(z_s - z_{S_n})$), because it depends upon the pathlength difference between the reference arm and the sample reflectors, that is, its position along the longitudinal axis. Notably, the square root dependence is a major gain factor with respect to direct detection of sample reflections. The "Auto-correlation term" stands for the interference between the different sample reflectors and represents a parasite signal. However, given the much smaller reflectivity of the sample reflectors compared to the reference reflectivity and the proximity between the sample reflectors, this component is usually overwhelmed by the cross-correlation term, and we will neglet it in the following treatment. One can easily see that the different reflections in the sample result in a modulation of the incoming spectrum, the amplitude and the frequency of which depend on the reflectivity of the sample reflectors and on its position, respectively. The fig. 2.2 shows examples for an outcoming spectrum and its relations with the physical parameters of the experimental setup.

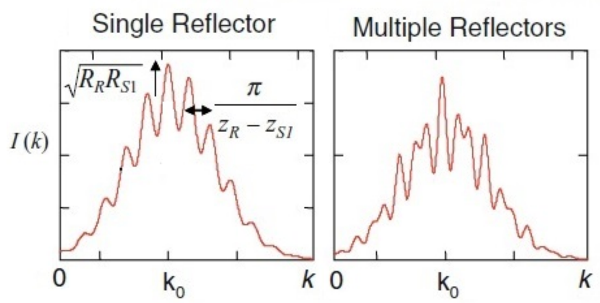

Figure 2.2: **OCM outcoming spectrum.** Left, spectral interferogram in the case of 1 single sample reflector; right, case of multiple sample reflectors. Adapted from [7]).

Fourier analysis is subsequently performed on the signal. By applying the Fourier transform to the intensity one obtains

$$\tilde{I}(z) = \mathcal{F}[I(k)](z) \propto \underbrace{\gamma(z)\left(R_R + \sum_n R_{S_n}\right)}_{\text{DC Term}} + \underbrace{\sum_n \sqrt{R_R R_{S_n}}\left[\gamma\left[2\left(z_R - z_{S_n}\right)\right] + \gamma\left[2\left(z_R - z_{S_n}\right)\right]\right]}_{\text{Cross-correlation Term}} \tag{2.2}$$

where $\gamma(z) = \mathcal{F}[S(k)](z) = e^{-z^2\Delta k^2}$. The sample reflectivity profile $\sqrt{R_S(z_s)}$ is then reproduced in the cross-correlation term: it has the shape of the illumination spectrum amplified by a factor of $\sqrt{R_R}$, appears double-translated with respect to the zero-reference position (i.e. z_R), and has a mirror-image at the opposite z-position. One can now easily see that some ways to improve the fidelity of the technique are to broaden the illumination bandwidth ($\Delta k \nearrow$) and to increase the reflectivity of the reference reflector ($R_R \nearrow$). Finally, in order to hide the large DC signal, one can measure the interference pattern without the sample and subtract it to the signal acquired in presence of the sample.

A main improvement of OCCS with respect to standard OCM is the possibility to get information about moving objects. After performing correlation analysis similar to that used in fluorescence correlation spectroscopy [14] (FCS), it has been shown that it is possible to characterize the motion of gold NPs in wells: the analysis was performed in the case of a radial zero-order Bessel illumination (the one used experimentally) and for freely-diffusing NPs[10]. If one considers more than one sampling volumes along the longitudinal axis, which is allowed by OCM with only one measurement, one can calculate the cross-correlation function $G_{mn}(\tau)$ of the fluctuating signals $I_m(\tau)$ and $I_n(\tau)$ in the sampling volumes V_m and V_n respectively

$$G_{mn}(\tau) = \frac{(T-\tau)\int_0^{T-\tau} I_m(t)\, I_n(t+\tau)\,\mathrm{d}t}{\int_0^{T-\tau} I_m(t)\,\mathrm{d}t \int_0^{T-\tau} I_n(t)\,\mathrm{d}t} - 1 \tag{2.3}$$

In the case of a net flow between the two sampling volumes, $\Delta G_{mn}(\tau) = G_m(\tau) - G_n(\tau)$ shows a non-zero amplitude with a maximum at $\tau = \tau_{mn}$, which is the mean transit-time for a NP from V_n to V_m. When $m = n$ the auto-correlation function describes the dynamics of particles within a sampling volume, which allows to obtain their concentration and their diffusion coefficient.

2.2 The experimental setup

In order to perform OCCS, we used several setups already present at the LOB.

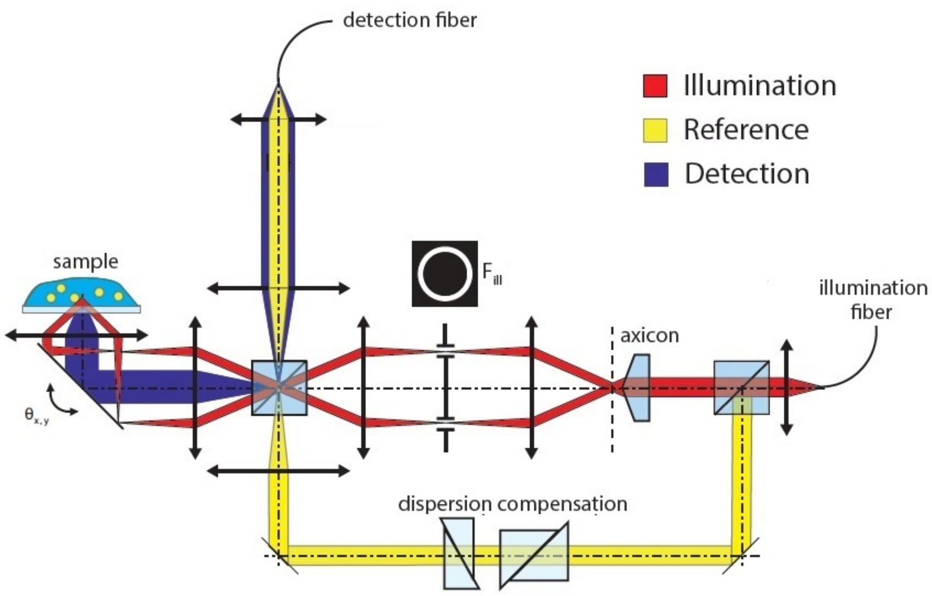

Figure 2.3: **xf-OCM (extended focus-optical coherence microscope).** Schematic of the setup for OCM. The illumination fiber brings the illumination light up to the entry lens; the detection fiber brings the detection light up to the spectrometer. The axicon serves to create a Bessel beam from the input Gaussian beam. A filter (F_{ill}) is used to cut some stray light from the tip of the axicon. Adapted from [10].

The first one we employed had a large working distance (WD >700 μm), a small detection numerical aperture (NA=0.22) and a large detection depht-of-field (DOF_d≈400 μm); this was in order for us to see deeply into the sample, which facilitates the detection of the gold NPs in the nanochannel of the Abionic chip[1]. This setup (fig. 2.3) implements an interferometer with an extra feature: the illumination does not have a Gaussian profile, but a zero-order Bessel profile; this means that its intensity is almost uniform along the propagation axis over most of our detection volume. The transformation of the input Gaussian beam into a Bessel beam is performed by the means of an axicon.

The second setup (WD<500 μm, NA=0.68 and DOF_d≈27 μm, fig. 2.4) is similar to the previous one, but it gives the possibility to further enhance the detection of gold NPs by using:

- the dark-field mode: a couple of filters (F_{ill} and F_{det}) is positioned in order to get rid of the illumination light that may be reflected due to the presence of the coverslide, which adds noise to the detection.
- the photothermal effect: when gold NPs are heated, they change the refractive index of the surrounding medium; this enhances the contrast and facilitates the detection of the scatters[2]. To make this

[1]The thickness of the pyrex piece of the Abionic chip is 500 μm, thus this is the minumum acceptable working distance to oserve the nanochannel for a close chip.

[2]For a detailed explanation of the model behind this phenomenon, one can refer to [9]

detection mode possible, the setup is equipped with several acousto-optical modulators (AOMs), which serve to modulate the illumination and the heating.

These two adjustements already improves the efficiency of the detection (i.e. in terms of signal-to-noise ratio).

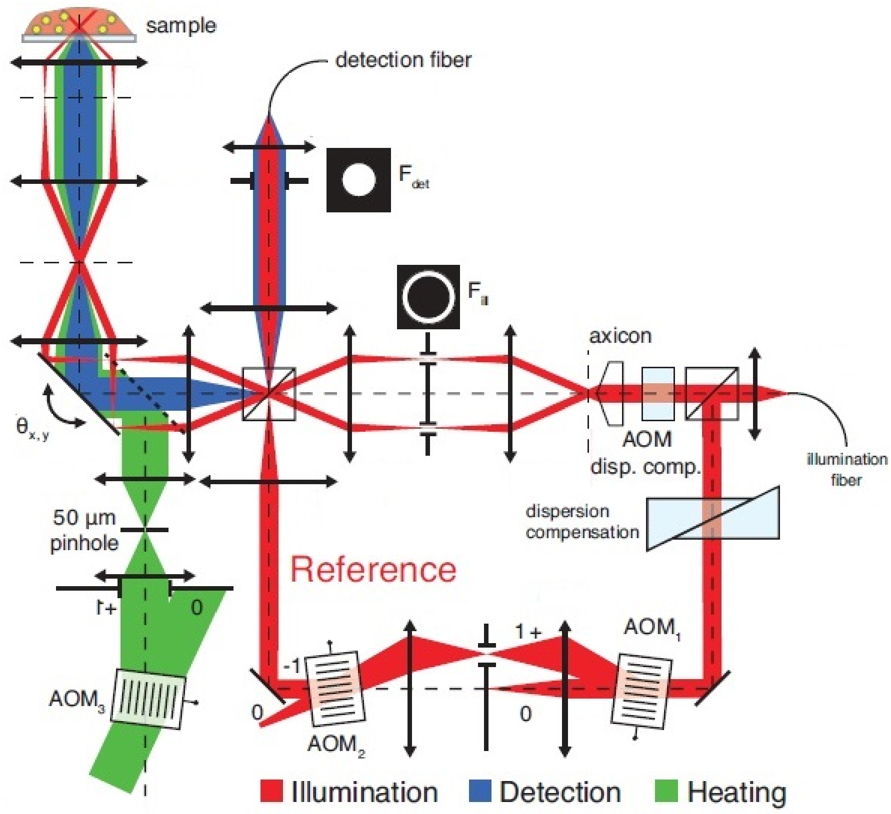

Figure 2.4: **df-OCM (dark-field optical coherence microscope).** Schematic of the setup for df-OCM. The setup is analogous to that shown in fig. 2.3, with additional filters (F_{ill} and F_{det}) to detect in the dark-field mode and additional acousto-optical modulators (AOMs) to perform OCM with photothermal effect. Adapted from [9].

Chapter 3

Results

3.1 Theoretical probing of the coating

An immunoassay is based on the specificity and the strength of the interaction between an antigen and its antibody: this has to be measured in the assay in order to detect the presence (and the amount eventually) of a specific antibody or antigen. With OCCS we are able to measure the diffusion coefficient of a gold NP. This parameter depends on the size of the diffusing object. When this changes, for example when other objects come to bind to the NP, we are able to measure this change: our idea is to coat the NP with an antigen, and to detect the presence of the specific antibody in the solution by using this effect on the diffusion. As a proof of concept, we decided to use 54kDa-streptavidin-coated NP and 150kDa-anti-streptavidin as antibody.

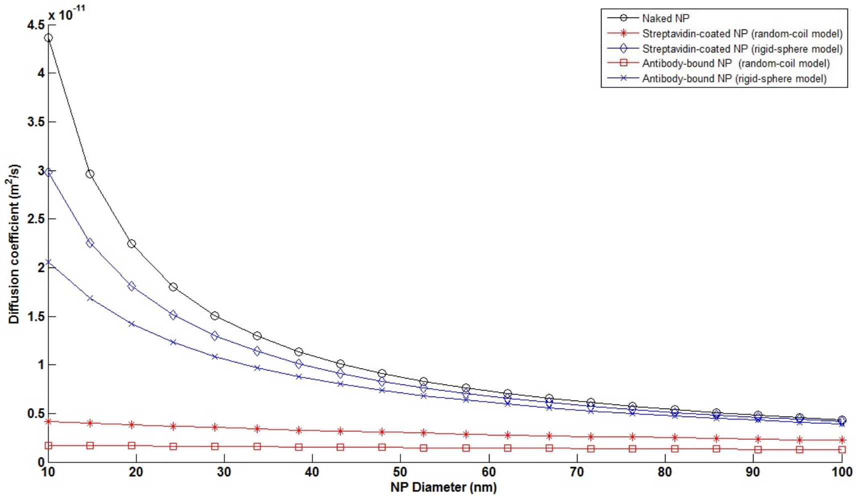

Figure 3.1: **Diffusion coefficient.** Numerical computation of the diffusion coefficient as a function of the NP diameter.

In this section we show the results from numerical computation to estimate the values of the diffusion coefficient for several situations (naked NP, coated NP, antibody-bound NP). We modelled the NP to being a rigid sphere, and the proteins to being either rigid spheres or random-coiled polymers. The model of proteins as rigid spheres considers the equivalent size of the protein to being the diameter of a homogenous sphere containing all the mass of the protein (protein mean density=1.35 g/cm^3[11], amino acid mean mass=110 Da). The model of proteins as random-coils considers the equivalent size to being the gyradius of a polymer having the same mass as the protein[1]. These are of course approximations, but give some idea about the range for the diffusion coefficients we expect to measure. A major limitation of this approach is to neglect the anisotropy of the structure, which is likely to occur in solution due to:

- intrinsic anisotropy of the shape of the NP[2],

[1] An empirical formula is used for globular proteins such as those used in our experiments and gives gyradius $= 7.257 + 0.395 * N^{\frac{3}{5}}$, where N is the number of amino acids in the protein[12].

[2] the supplier declares a CV<12% for its streptavidin-coated NPs.

- inhomogeneous coating,
- inhomogeneous antibody binding.

In order to enhance the difference in the diffusion coefficient between the coated and the antibody-bound NP, the only three free parameters we have for optimization are the size of the NP, the temperature and the viscosity of the medium. Changing the characteristics of the medium is not a good idea, because both the temperature and the viscosity may affect the native structure of the proteins, by preventing their interactions or creating artefacts. Therefore, we computed the diffusion coefficients as a function of the NP diameter. Fig. 3.1 shows the diffusion coefficients of the three structures mentioned above as a function of the NP diameter. As one can easily see, the two models give quite different results. Since the rigid-spheres and the random-coils model are the most and less restrictive in terms of size of the proteins, respectively, we expect to measure values within these two limits. We next calculated the relative shift of the diffusion coefficient calculated as $\left|\frac{D_{\text{Antibody-bound}}}{D_{\text{Coated}}} - 1\right|$: this parameter allows to find the range within which we are able to discriminate the diffusion of an antibody-bound NP and a simple coated NP. Fig.

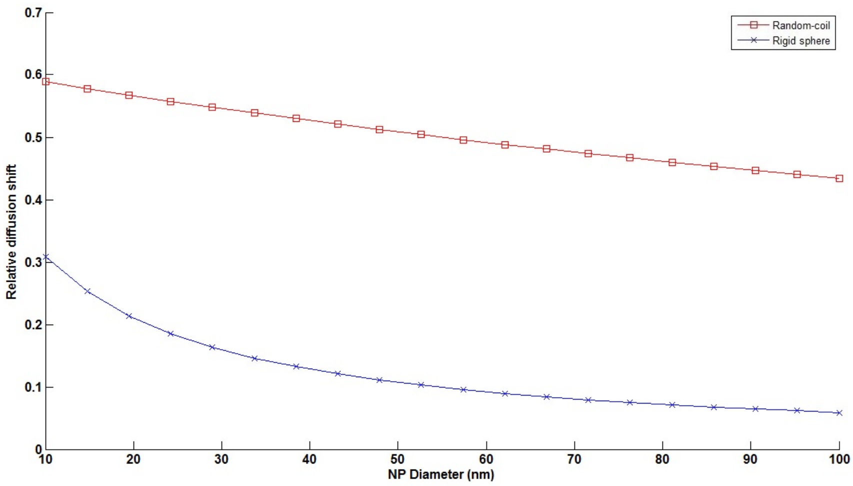

Figure 3.2: **Relative diffusion shift.** Numerical computation of the relative diffusion shift as a function of the NP diameter.

3.2 shows that in the ideal situation with homogenous coating and binding, in the frame of random-coil model, we would be able to obtain a relative shift up to 40-60% in the range of NP size available. Much less this would be in the case of rigid-spheres (10-20%). We finally want to mention that what we have computed here is only the (theoretical) mean value of the distribution of the diffusion coefficient measured during an experiment. The standard deviation should be calculated by taking into account: variations in the shape of the NP and the proteins, the non-homogeneity in coating and binding. We do not have enough data at this point to be confident on a calculation of this parameter.

3.2 Study of gold NPs with xf-OCM

The first step of our project was to find a way to detect the gold NPs once injected into the Abionic chip. We wanted to use the xf-OCM to exploit its larger working distance to be able to look into the nanochannel. Since the previous studies[9, 10] had been done with gold NPs in wells of plastic and on the df-OCM, we first wanted to assess the reliability of the new setup with the same sample before passing to the analysis in the sensor.

We prepared a 9.3pM solution of gold NPs (ø=80 nm) in ultrapure water. We put it into a well and performed OCM with the xf-OCM. An example of what we obtained is shown in fig. 3.3. As one can see, the SNR is high enough only to clearly identify the air-water interface, which is a powerful reflector. No putative NP could be identified over the background noise. As a comparison, fig. 3.4 shows results from the same method with the same sample characteristics (i.e. concentration, NPs diameter) but using the df-OCM. The gold NPs are clearly visible in the colour-coded image and their signal appears very peaked over the background. The probable explanation for such a behaviour is that the NA of the xf-OCM is almost 1/3 of that of the df-OCM, thus the signal collected is much lower, resulting in a much worse SNR. For this reason we have chosen to come back to the df-OCM for the further studies.

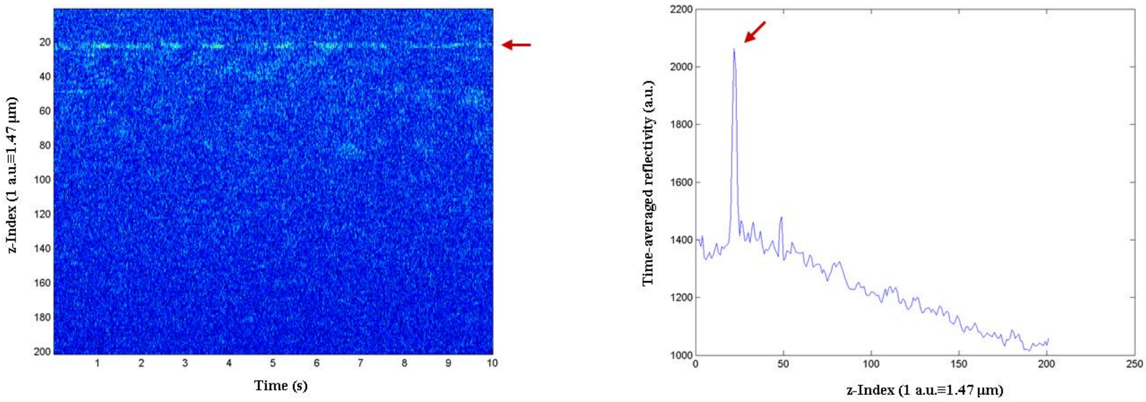

Figure 3.3: **NPs in a well with xf-OCM.** Results of OCM after Fourier analysis. Left: colour-coded reflectivity as a function of depth in the sample (vertical axis) and time (horizontal axis). Right: time-averaged reflectivity profile as a function of the depth in the sample (z-index). Red arrows indicate the air-water interface.

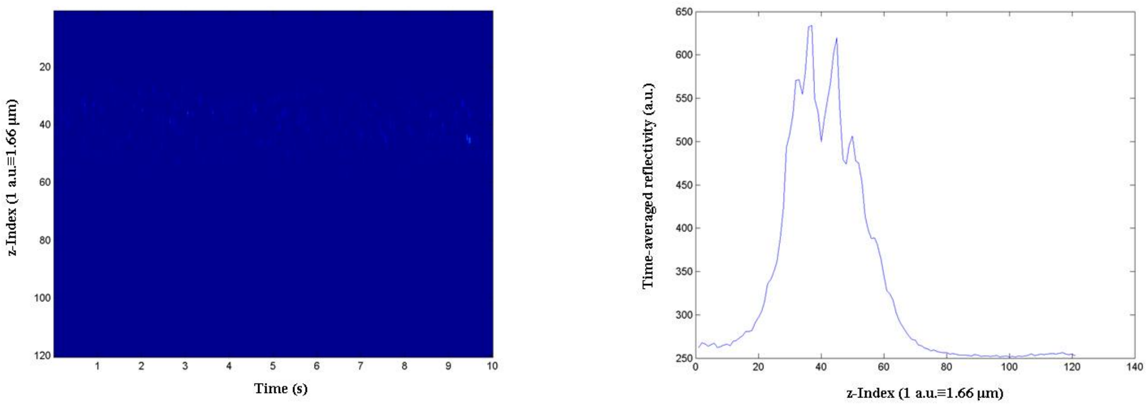

Figure 3.4: **NPs in well with df-OCM.** Results of OCM after Fourier analysis. Left: colour-coded reflectivity as a function of time and depth in the sample (z-index). Right: time-averaged reflectivity profile as a function of the depth in the sample (z-index). These images come from measurements performed by Stéphane Broillet, PhD candidate at the LOB.

3.3 FCS on gold NPs

Since the df-OCM was under repair for long, we used an experimental setup allowing to perform FCS measurements to test the possibility to observe a variation in the diffusion coefficient of gold NPs by the means of bound antibodies. As we wanted to have the largest variation in the diffusion coefficient (the smaller the NP, the more the variation) but we did not know how much signal we would have obtained with the OCCS setup (the bigger the NP, the larger the signal), we used intermediate 50nm-NPs, for which we expected a relative variation of the diffusion coefficient between 10% and 50% (fig. 3.2), depending on the efficiency of the coating and of the antibody binding.

Two lasers were available on the setup (488 nm and 633 nm), but only the 488 allowed us to have a fluorescence signal from the gold NPs. For this reason, we will only discuss this case. So as to calibrate the instrument, to find the good position of the focus and of the pinhole, and also to have a reference value for the diffusion coefficient, we used a solution of 50nM Atto488 diluted in PBS pH7.4 (time-trace, autocorrelation and fit from one measurement are shown in fig. 3.5). We used the following formula[14] for fitting the autocorrelation data between 10 ms and 10 s[3]:

$$G(\tau) = \frac{1}{\langle N \rangle} \frac{1 - F + Fe^{-\tau/\tau_F}}{1 - F} \frac{1}{\left(1 + \frac{\tau}{\tau_D}\right)\left(1 + \frac{\tau}{a^2 \tau_D}\right)^{0.5}} + G(+\infty) \tag{3.1}$$

Where $\langle N \rangle$ is the mean number of fluorophores in the confocal volume, F the fraction of fluorophores in

[3]The values of the autocorrelation curve are not reliable below 10 ms; see appendix B and fig. 3.7

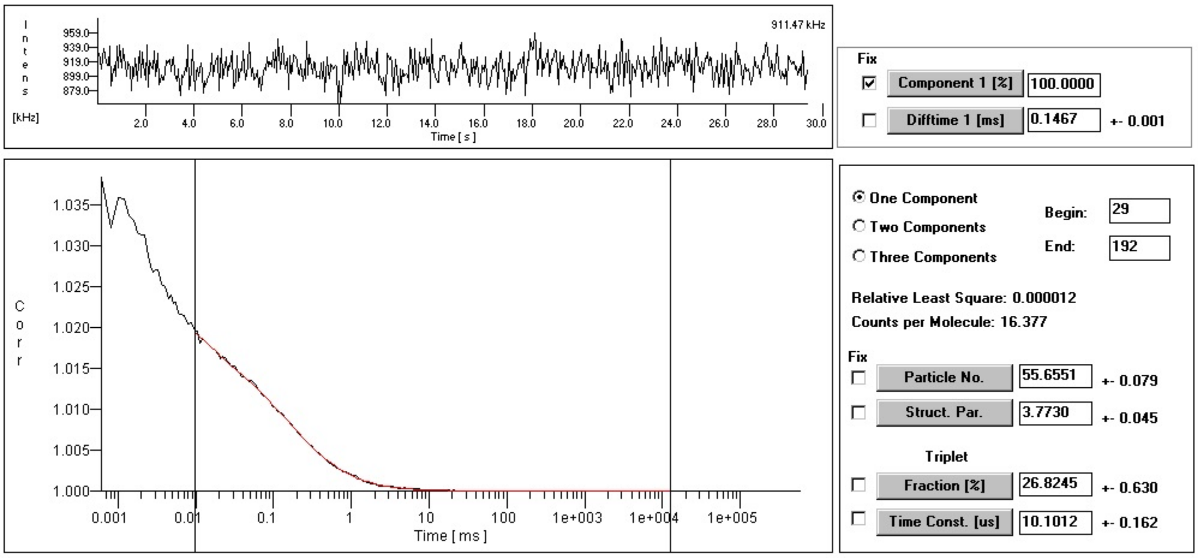

Figure 3.5: **FCS Atto488 50nM.** Left, time-trace of Atto488 fluorescence (top) and autocorrelation curve (bottom); right, parameters from the fit (red line in the autocorrelation graph).

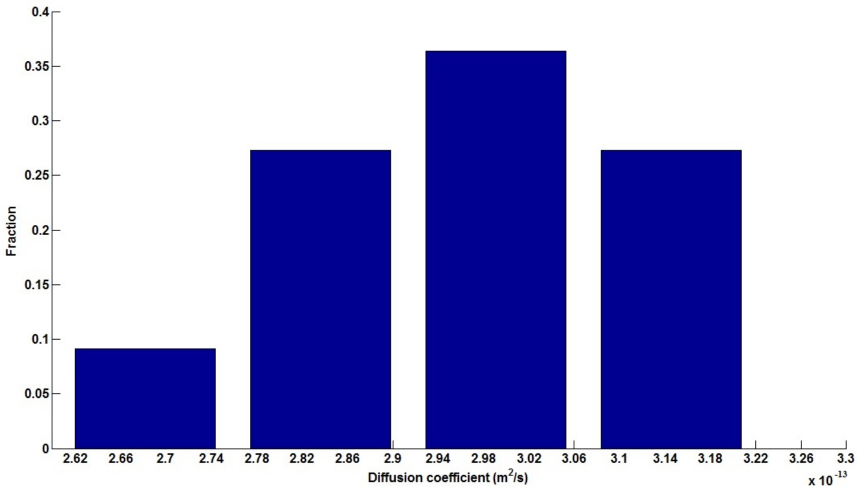

Figure 3.6: **Distribution of the diffusion coefficient of Atto488.** Distribution of the diffusion coefficient for a solution of 50 nM of Atto488. (3.0±0.2)*10^{-13} m^2/s (n=11).

the triplet state, τ_F the relaxation time of the triplet state, τ_D the diffusion time of the fluorophores, and a the structure parameter of the confocal volume[4]. We measured a number of molecule of 50.69±2.80 (n=11) within the confocal volume and a structure parameter of 5.10±0.97 (n=11); this allowed us to estimate the spot size in the lateral dimension (≈390 nm) and to calculate the diffusion coefficient. The distribution of this parameter for Atto488 is shown in fig. 3.6.

This calibration step served to fixe some other parameters to determine the diffusion time for 74pM 50nm-NPs (time-trace, autocorrelation and fit of one measure are shown in fig. 3.7). The distribution of the diffusion coefficient is shown in fig. 3.8. One can easily see the much broader distribution with respect to that of Atto488. A broad distribution may prevent from distinguishing between two different species of NPs (coated vs non-coated or antibody-bound vs coated).

Therefore, we next analyzed a sample containing 50pM streptavidin-coated 50nm-NPs. Unfortunately, the fitting did not work for this sample (fig. 3.9): as one can see in the time-trace, there is a higher fluorescence intensity from the sample than there is with non-coated NPs. The reasons for this could be several:

- the coating changes the spectral properties of the gold NPs;

[4]This is the ratio of the longitudinal size to the lateral size.

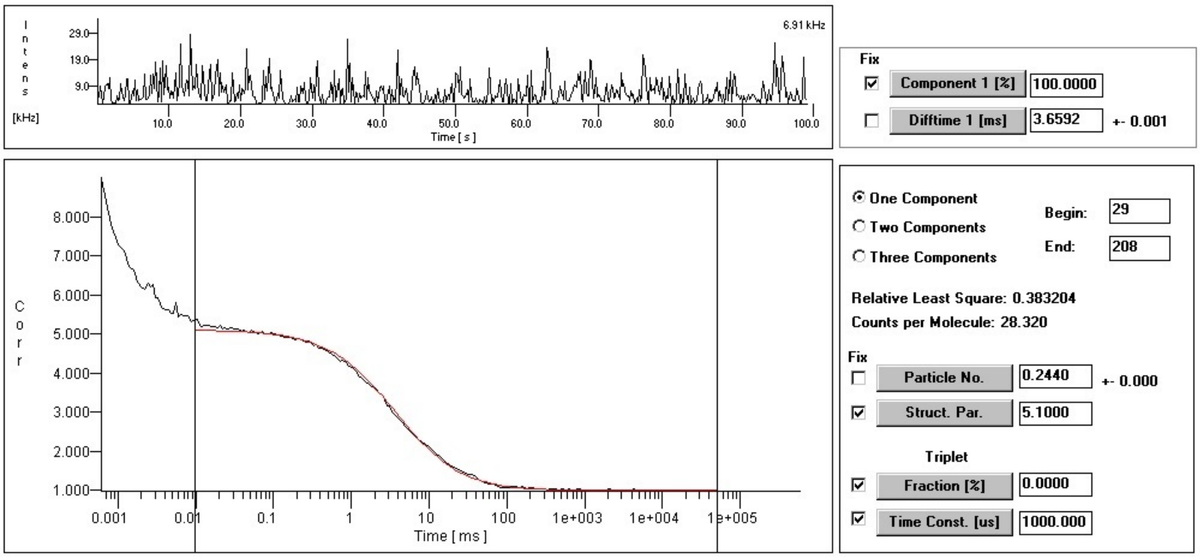

Figure 3.7: **FCS 50nm-NPs 74pM.** Left, time-trace of NPs fluorescence (top) and autocorrelation curve (bottom); right, parameters from the fit (red line in the autocorrelation graph).

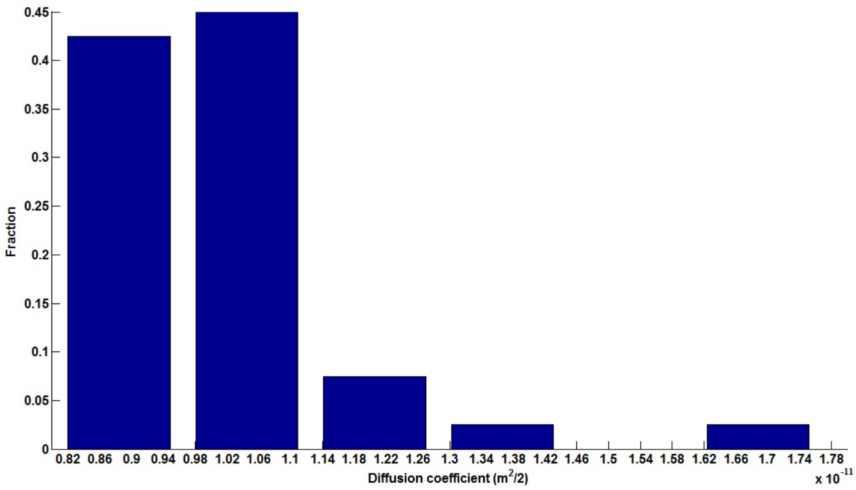

Figure 3.8: **Distribution of the diffusion coefficient of gold NPs.** Distribution of the diffusion coefficient for a solution of 74 pM of 50nM-NPs. $(1.0 \pm 0.2) * 10^{-11}$ m^2/s (n=40).

- there is some other component that fluoresces in the solution;
- there is some component in the solution that makes some but not all the gold NPs more fluorescent (e.g. because it is not homogenous within the solution).

We did not inspect the problem in detail because this was out of the focus of this project, but we believe glycerol to be a putative responsible for this phenomenon:

- it can be used to increase fluorescence of gold NPs[15];
- we found that a solution of 100% glycerol gives a fluorescent signal when studied with our setup and parameters (see appendix fig. B.2);
- since we have ≈6% of glycerol in the solution with coated-NPs, this may give a parasite signal, preventing from a good fitting.

Anyway, it was not possible to obtain reliable values for the diffusion coefficient of coated-NPs. Therefore we came back to OCCS.

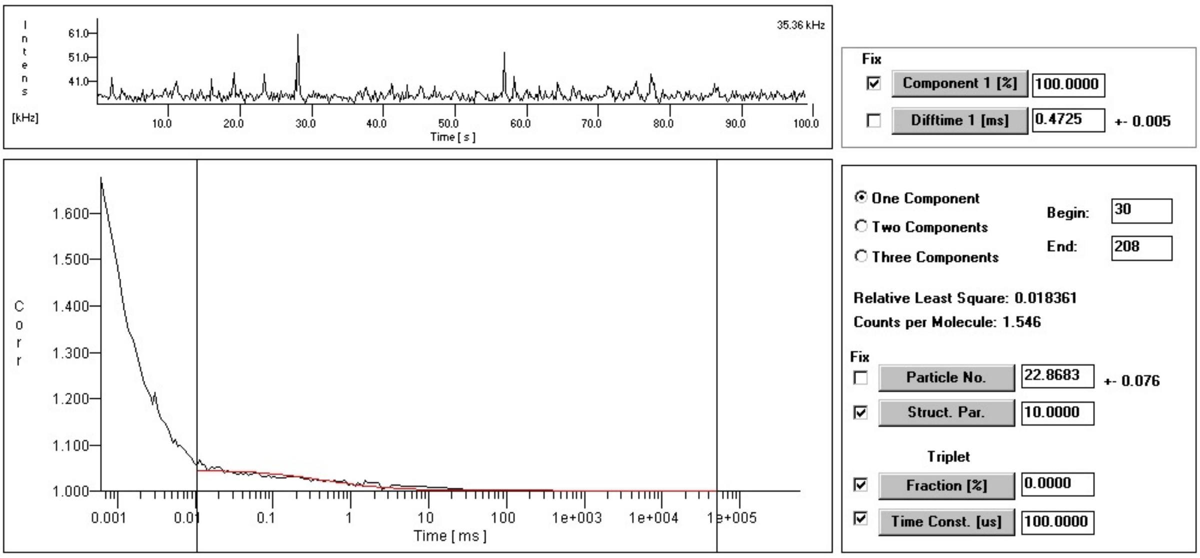

Figure 3.9: **FCS coated-NPs 50pM.** Left, time-trace of coated-NPs fluorescence (top) and autocorrelation curve (bottom); right, parameters from the fit (red line in the autocorrelation graph).

3.4 OCCS on gold NPs

Detection and fitting

As a proof of concept of OCCS for immunoassays, we tested the possibility to detect a shift in the diffusion coefficient for bare gold NPs (bNPs) and strepatividin-coated gold NPs (cNPs), in presence of several concentrations of either anti-streptavidin or anti-β-lactoglobulin (used as a negative control). Both cNPs and bNPs were tested at a concentration of 10pM, but the former were buffered in PBS pH7.4 and 1.7% glycerol (v/v), whereas the latter were in ultrapure water and 1.7% glycerol (v/v)[5].

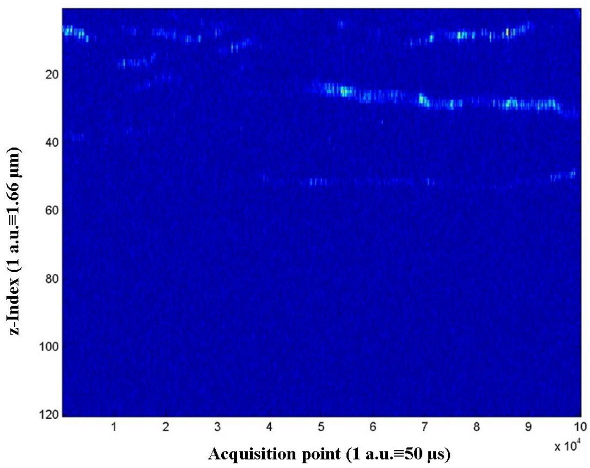

Figure 3.10: **Tomogram from df-OCM.** Colour-coded reflectivity as a function of the acquisition point (equivalent-time) and depth in the sample (z-index) for 10pM cNPs.

We used the df-OCM to perform these analysis, by shining with a near-infrared laser giving a final power of ≈2 mW to the sample[6]. For each measurement, we deposited a 30µL droplet containing NPs in a plastic well and closed it to prevent evaporation. For the measurements in the presence of an antibody,

[5]The solution of cNP is supplied in PBS pH7.4 and 20% glycerol; thus, we adjusted the concentration of glycerol for the bNPs solution in order to get the same viscosity. We used ultrapure water for bNPs because they displayed a strange behaviour when buffered in PBS.

[6]This power is much enough to obtain a signal from the scattering NPs without pushing them along the longitudinal axis.

we added 2µL of it in order to obtain the desired final dilution for the antibody[7]. We always made acquisition with an integration time of 50µs and over (only) 5s: this was a major limitation due to a technical problem in the acquisition card and may have decreased the goodness of the fit.

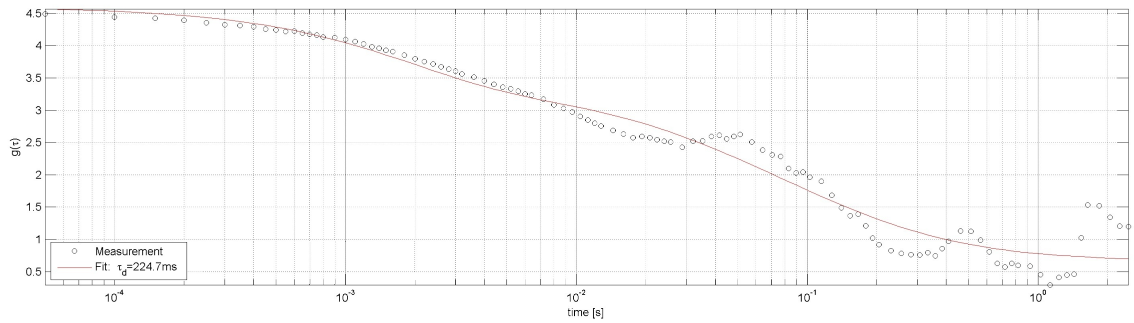

Figure 3.11: **Correlation curve.** Autocorrelation of the reflectivity signal as a function of the lag-time for the tomogram in fig. 3.10. Fitted curve is shown in red: fitted diffusion time is indicated in the legend.

Fig. 3.10 shows a tomogram resulting from one of the measurements we performed on cNPs. One can easily notice the difference in terms of SNR with respect to fig. 2.3, obtained with the xf-OCM. We could then use the tomograms to calculate the correlation curves for different sampling volumes; this increased the statistics and made our values for the diffusion coefficient more reliable. One autocorrelation curve is shown in fig. 3.11. For large lag-time, the curve is not smooth but presents peaks and valleys: this is probably due to the short measurement time used for the acquisition, because it is present also for bNPs, which was not the case in previous measurements.

The measured values of the number of particles in the sampling volume is shown in fig. 3.12. When a coating and/or an antibody is added to the bNPs, there is a slight increase of this parameter and its variations. After statistical analysis (Mann-Whitney U-test) we obtained that:

- bNPs and cNPs are statistically different ($p<0.05$);
- the addition of 42nM of anti-streptavidin to cNPs does not make changes with respect to the absence of antibody in the solution ($p=0.84$), but it does a bit when adding less concentrated solutions ($0.10<p<0.20$).

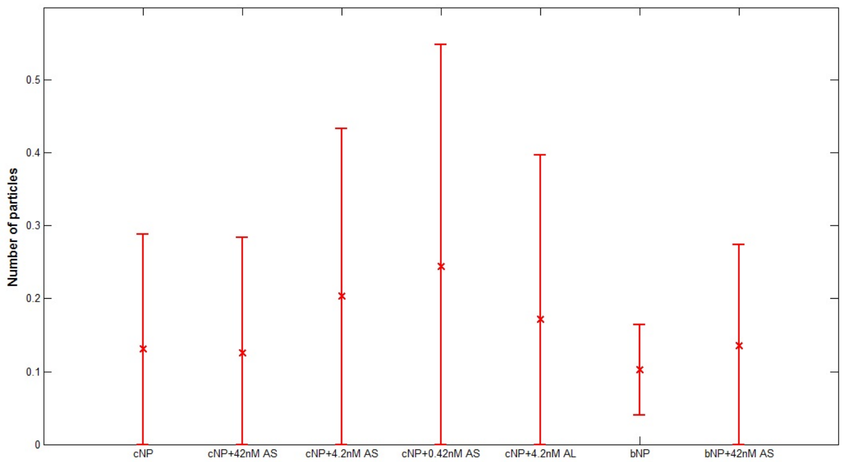

Figure 3.12: **Number of particles in the sampling volume.** Fitted number of particles for the conditions studied with OCCS (bNP=bare-NP, cNP=coated-NP, AS=anti-streptavidin, AL=anti-β-lactoglobulin).

Distributions of the diffusion coefficients

The first question we wanted to address was how the presence of the streptavidin coating around the NPs influenced their motion. Fig. 3.13 shows the distributions of the diffusion coefficient for bNPs and

[7] We did not consider the variation of the concentration of the NPs (<6%).

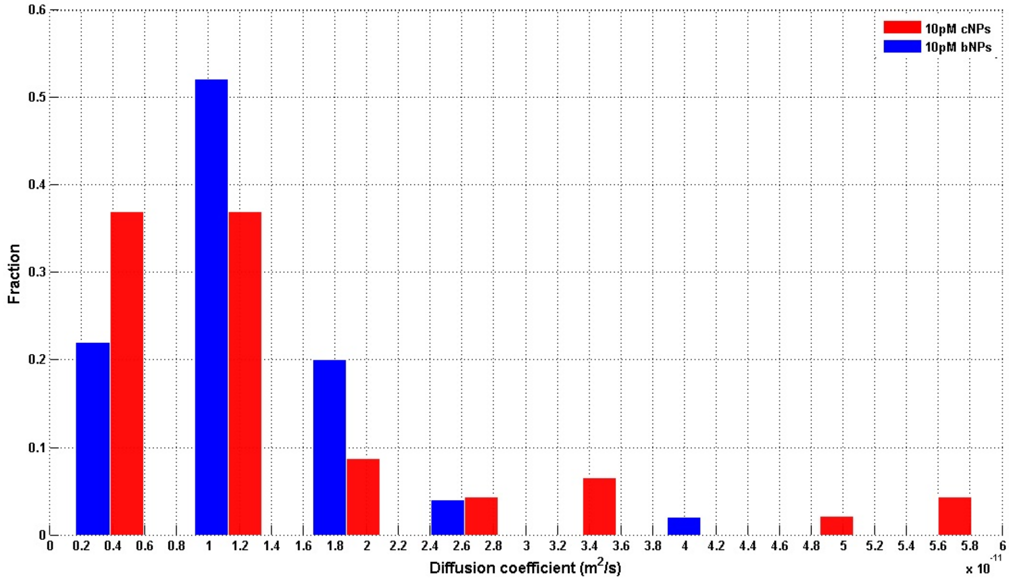

Figure 3.13: **Effect of the coating on diffusion.** Distribution of the diffusion coefficient for a solution of 10pM of bare-NPs and coated-NPs.

cNPs. Despite a relative diffusion-shift of $\overline{D}_{\mathrm{cNP}}/\overline{D}_{\mathrm{bNP}} - 1 = +0.16$, the two distributions are mainly superimposed and there is no possibility to distinguish one from each other (p=0.22, Mann-Whitney U-test). Importantly, the distribution for cNPs is broader than that for bNPs: this may be due to inhomogeneity in the coating, which generates particles with different hydrodynamic radii[8].

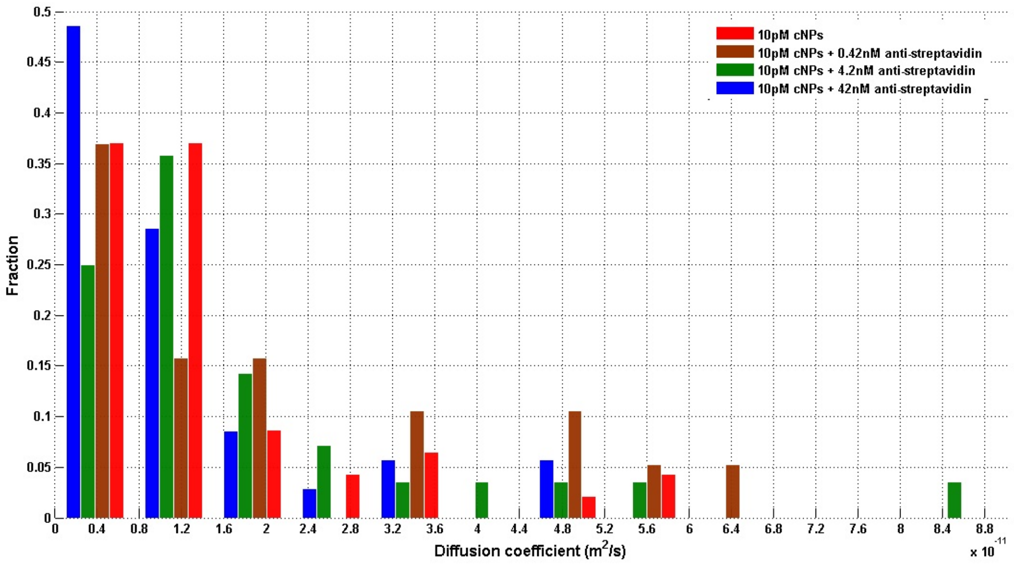

Figure 3.14: **Effect of the specific antibody on diffusion.** Distribution of the diffusion coefficient for a solution of 10pM of coated-NPs in presence of the indicated concentration of anti-streptavidin IgG.

The point in immunoassays is to be able to distinguish situations where a specific antibody is present in the solution from those where it is not (and eventually to quantify its concentration). Therefore, we tested the diffusion of cNPs in presence of several concentrations of anti-streptavidin (fig. 3.14): 0nM, 0.42nM, 4.2nM, 42nM (which correspond to 0X, 42X, 420X, 4200X the concentration of gold NPs respectively). This serial dilution was chosen in order to cover 1 order of magnitude around the value that saturates the sites on the NPs. The measured relative diffusion-shifts with respect to cNPs (0X) are: +0.51 (42X), +0.35 (420X), -0.17 (4200X). Once again, all the distributions are partially superimposed, but some considerations can be made:

[8] In fact, the supplier argues ≈400 sites on a single NP, but no real test neither quantitative information is given.

- addition of only 42X of specific antibody already broadens the distribution with respect to the case with 0nM;
- the 4200X solution has the narrowest distribution and the highest shift towards the low values of the diffusion coefficient;
- the distributions with 0.42nM and 4.2nM are almost identical (p=0.87, Mann-Whitney U-test) and both are quite different from the one with 42nM (p<0.06, Mann-Whitney U-test);
- the distribution with 0nM is not statistically very different from the others (0.13<p<0.26, Mann-Whitney U-test).

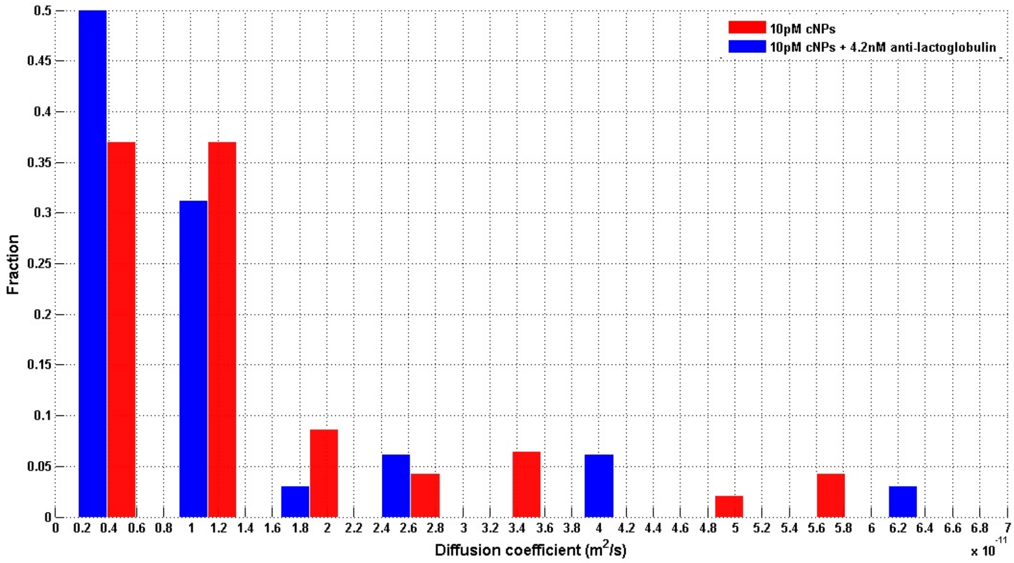

Figure 3.15: **Effect of the non-specific antibody on diffusion.** Distribution of the diffusion coefficient for a solution of 10pM of coated-NPs in presence of anti-β-lactoglobulin IgG.

In order to verify the specificity of the interaction between the cNPs and the antibodies, we measured the diffusion coefficient in the presence of a non-specific antibody, the anti-β-lactoglobulin, which is not expected to recognize the coating of the NPs. Fig. 3.15 shows that may be a non-specific interaction between the NPs and the antibody, because the distribution shifted towards lower values for the diffusion coefficient after addition of 4.2nM of anti-β-lactoglobulin; the measured relative diffusion-shift (-0.13) seems to confirm this fact. However, the p-value (p=0.18, Mann-Whitney U-test) suggests that the two distributions are not statistically very different.

Since it seemed to be a non-specific interaction between the antibody and the NPs, we further investigated this aspect by adding 42nM of anti-streptavidin to a solution of bNPs (fig. 3.16). Despite a very small relative diffusion-shift $\overline{D}_{42\text{nM}}/\overline{D}_{\text{bNP}} - 1 = -0.04$, the presence of the antibody seems to slightly left-shift and broaden the distribution (p=0.05, Mann-Whitney U-test) and we finally suspect that a small non-specific interaction may occur in this case.

Fig. 3.17 shows a comparison of all the distributions for the different conditions studied.

3.5 Discussion

We tried to give a proof of concept of OCCS to perform immunoassay, by employing gold NPs as physical reporters of the interaction between an antigen coated on their surface and a free antibody in the solution. This was in preview of translating this method into the Abionic chip, the industrial partner for this project.

As a first step, we estimated the potential change in the diffusion coefficient of different kinds of NPs (bare vs streptavidin-coated), in the presence/absence of a specific antibody, and for two models for the structure of a protein (sec. 3.1). We obtained a shift of the diffusion coefficient that was very different between the several cases and dependent on the NP radius. We sought to characterize the immunoassay in well-plates, by using FCS and OCCS. We have chosen 50nm-NPs as a compromise between a good SNR in OCCS and a good (theoretical) diffusion-shift.

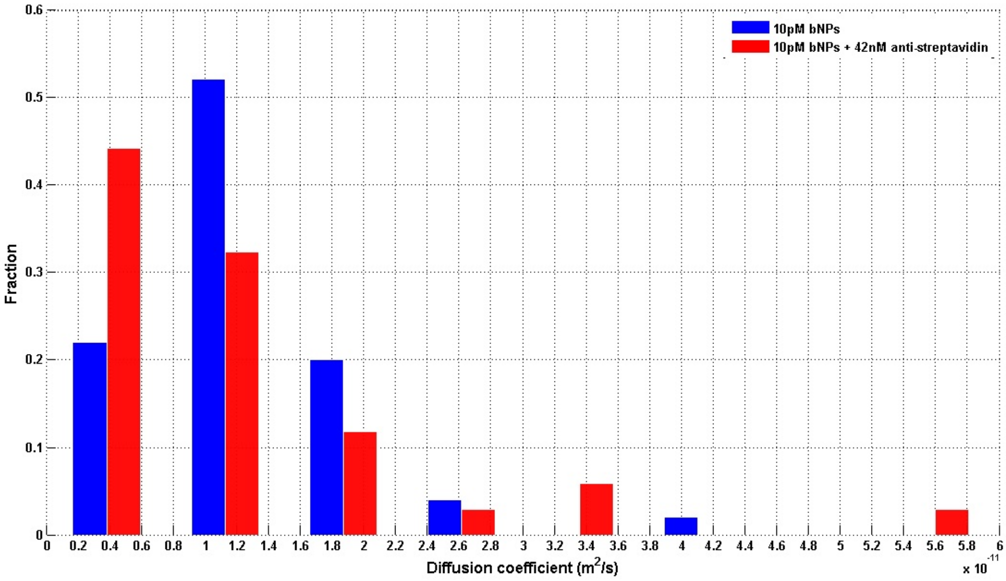

Figure 3.16: **Effect of the antibody on diffusion of non-coated NPs.** Distribution of the diffusion coefficient for a solution of 10pM of bare-NPs in presence of anti-streptavidin IgG.

In FCS measurements (sec. 3.3), after calibration of the experimental features and the fitting parameters with Atto488, we found that the diffusion coefficient of bNPs was exactly the one we would expect theoretically. Regrettably, the same measurement for cNPs did not work, preventing us from further confirmation of our analytical predictions. We argue that the presence of glycerol in the buffer generates artefacts which interfere with our fluorescence measurements.

In OCCS measurements (sec. 3.4) we found that the presence of the streptavidin coat increases the number of NPs in the sampling volume as if their concentration were higher. This may be due to interactions between NPs, which would cause their retention within the sampling volume. If this were the case, the free-diffusion model would not hold any more and the values obtained for the diffusion coefficient would not be reliable. Another explanation of the observed behaviour could be the fact that the short measurement time (only 5 seconds) does not allow a large statistics for the fitting step, and generates fictive larger variations. However, we always remained in the "single particle" regime, with less than 1 NP in the sampling volume[10]. Interestingly, the addition of small quantities of specific antibody increases the number of particles in the sampling volume and its variations much more than when adding large amounts. This can be explained by the fact that when adding quantities of antibody that are less than the saturating concentration (which is the case for the 42X and 420X solutions), the solution will be depleted rapidly and the cNPs will be covered very differently one from each other (in particular, those being close to the point of injection of the antibody will be much more covered than the farther ones). This creates different species of NPs in the solution and, once again, a more detailed model should be envisaged to describe their dynamics. Conversely, when the concentration of the antibody is much enough to saturate the sites on the cNPs (which is the case for the 4200X), the NPs will be covered more homogenously. An aspect we did not addressed was the effect of molecular crowding[16]: a large amount of small objects (e.g. antibodies) in a solution with bigger objects (e.g. NPs) tends to make the latter get statistically closer and even to agregate. However, for our values for the size of the objects and the concentrations, we estimated the entropic forces to be «1 fN, which is completely negligible.

Concerning the distributions of the diffusion coefficient, we obtained values coherent with the theoretical estimation and the FCS measurements. We found that bNPs and cNPs are mainly undistinguishable, which is in contrast with results from the previous analysis on the number of particles in the sampling volume. This makes us more confident on the hypothesis that it was an artefact due to the short measurement time rather than an interaction between cNPs: if so, we would expect a decrease in the diffusion coefficient as well, which is not the case here (we conversely observe an increase of the diffusion coefficient for cNPs). Once again, small concentrations of antibody showed to have larger influences on the distribution than do larger concentrations. 4200X solution was the one with the narrowest distribution and higher decrease, which confirms that the presence of the specific antibody affects the motion of cNPs. With the few values of the concentrations tested and the presence of the artefacts described above

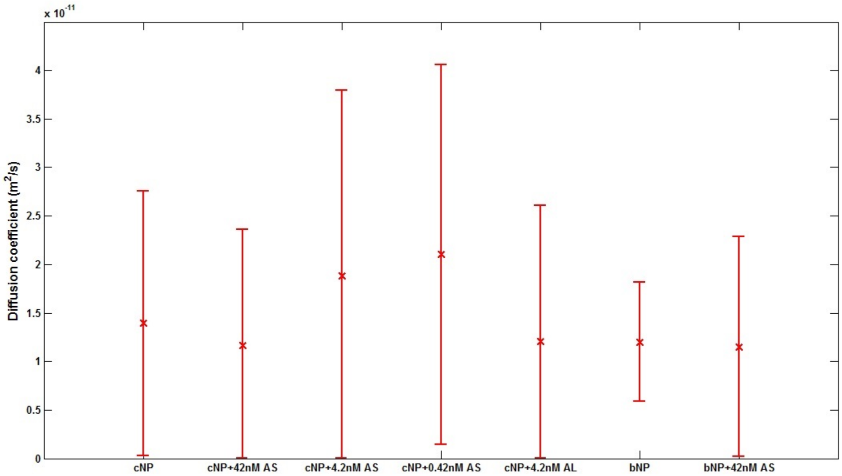

Figure 3.17: **Diffusion coefficient of gold NPs.** Fitted diffusion coefficient for the conditions studied with OCCS (bNP=bare-NP, cNP=coated-NP, AS=anti-streptavidin, AL=anti-β-lactoglobulin).

we could not really find a relation between the concentration of the specific antibody and the resulting diffusion coefficient. Moreover, we found almost the same diffusion-shift as with 4200X anti-streptavidin by studying the motion of cNPs in presence of 420X anti-β-lactoglobulin. Statistical analysis suggested that this value is not statistically relevant but further analysis should be done: for instance, a larger concentration should be tested before concluding definitively[9]. Still, we found a putative non-specific interaction between bNPs and 4200X anti-streptavidin, which can cause erroneous detection when applied to real case diagnostic. This point, which can be due to the fact that the main body on the antibodies (Fc part) is prone to unspecifically bind to external elements, would deserve further investigation as well.

However, all the previous results were obtained with large variations between the measurements, thus one should not consider them as conlusive but as indications for future analysis.

[9]The stock solution we had for the anti-β-lactoglobulin did not allow to have concentrations above 4.2nM.

Chapter 4

Conclusion

In the frame of this project, we aimed to apply a novel optical technique to immunoassays. The Laboratory of Biomedical Optics has developed a method that takes advantage from the synergy of Optical Coherence Microscopy and correlation analysis: this is called Optical Coherence Correlation Spectroscopy. In particular, this technique allows to determine the diffusion coefficient of gold NPs that freely diffuse in solution. By exploiting the interaction between an antigen coated on their surface and its specific antibody in solution, one can envisage to measure the change in the diffusion coefficient to verify, and sometimes quantify, the presence of a specific antibody in blood sample. We tested this detection mode in solution:

- the presence of a streptavidin-coat on the surface of 50nM gold NPs does not seem to affect their diffusion coefficient;
- the presence of anti-streptavidin in solution with coated-NPs affects their diffusion coefficient dependently on the concentration of the antibody, with smaller ones having a more visible effect than higher ones;
- a non-specific interaction between the antibodies and the gold NPs may occur and change their diffusion motion.

A major problem in our measurements was the large variation obtained for the parameters studied. For this, it would be interesting to perform further assays with smaller NPs: the new poli-OCM setup available at the LOB has an increased sensitivity due to the use of the photothermal absorption[17], which would limit the detection to NPs only in the sample and would allow to detect smaller NPs. This will increase the diffusion-shift and make the distributions narrower because of the less antigen sites on the surface of the NPs. Moreover, the surface available for non-specific binding would decrease as well. All together, these features would subsequently push the detection limit down, and this could be a powerful means to diagnose allergies. Previous tries to integrate immunoassays based on optical detection of gold NPs on-chip have proven the potential of such devices[18]. A solution for studying the motion of gold NPs in nanochannels could be to fabricate PDMS chips with similar sizes. Furthermore, the possibility that PDMS offers to easily vary the dimensions of the reaction channels will give the chance to find an optimum for the concentration and size of gold NPs for a sensitive detection of antibodies. Importantly, what remains to test and optimize is the use of the specific advantage of OCCS with respect to other optical techniques: the opportunity to probe several sampling volumes simultaneously and to find directional motions by the means of correlation analysis (fig. 4.1).

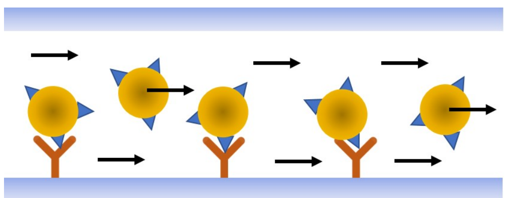

Figure 4.1: **Alternative way to perform immunoassay with OCCS.** Schematic of a nanochannel where the quantification of antibody-antigen binding is given by the difference in flowing velocity of NPs instead of difference in diffusion coefficient.

Bibliography

[1] *Commercialization of microfluidic point-of-care diagnostic devices.* C. D. Chin, V. Linder and S. K. Sia. **Lab Chip, 2007, 7 , 41–57**.

[2] *Point-of-Care Diagnostics for Global Health.* P. Yager, G. J. Domingo and J. Gerdes. **Annu. Rev. Biomed. Eng. 10:107–44, 2008**.

[3] *Electrical detection of single viruses.* F. Patolsky, G. Zheng, O. Hayden, M. Lakadamyali, X. Zhuang and C. M. Lieber. **PNAS, September 28, 2004, Vol. 101, No. 39**.

[4] *Enzyme-linked Immunosorbent Assay (ELISA).* Dr. G. Chandra. **www.iaszoology.com/elisa**.

[5] *Indirect competitive immunoassay for the detection of fungicide Thiabendazole in whole orange samples by Surface Plasmon Resonance.* M. C. Estevez, J. Belenguer, S. Gómez, J. Miralles, A. M. Escuela, A. Montoya and L. M. Lechuga. **Analyst. 2012 December 7; 137(23)**.

[6] *Optical imaging techniques for point-of-care diagnostics.* H. Zhu, S. O. Isikman, O. Mudanyali, A. Greenbaum and A. Ozcan. **Lab Chip, 2013, 13, 51**.

[7] *Optical Coherence Tomography.* J. A. Izatt and M. A. Choma. **Springer, Chapter 2, 2008**.

[8] *Localized Surface Plasmon Resonance Spectroscopy and Sensing.* K. A. Willets and R. P. Van Duyne. **Annu. Rev. Phys. Chem. 2007. 58:267–97**.

[9] *Fast three-dimensional imaging of gold nanoparticles in living cells with photothermal optical lock-in Optical Coherence Microscopy.* C. Pache, N. L. Bocchio, A. Bouwens, M. Villiger, C. Berclaz, J. Goulley, M. I. Gibson, C. Santschi and T. Lasser. **Optics Express 21385, Vol. 20, No. 19, September 2012**.

[10] *Optical Coherence Correlation Spectroscopy (OCCS).* S. Broillet, A. Sato, S. Geissbuehler, C. Pache, A. Bouwens, T. Lasser and M. Leutenegger. **Optics Express, Vol. 22, Issue 1, 782-802, 2014**.

[11] *Average protein density is a molecular-weight-dependent function.* H. Fischer, I. Polikarpov and A. F. Craievic. **Protein Sci. 2004 October; 13(10): 2825–2828**.

[12] www.scfbio-iitd.res.in/software/proteomics/rg.jsp.

[13] *Spectroscopic Optical Coherence Tomography and Microscopy.* A. M. Oldenburg, C. Xu and S. A. Boppart. **IEEE journal of selected topics in quantum electronics, Vol. 3, No. 6, November/December 2007**.

[14] *Fluorescence correlation spectroscopy. An introduction to its concepts and applications.* P. Schwille and E. Haustein. **Biophysics Textbook Online, 1, No. 3, 2001**.

[15] *Making gold nanoparticles fluorescent for simultaneous absorption and fluorescence detection on the single particle level.* A. Gaiduk, P. V. Ruijgrok, M. Yorulmaz and M. Orrit. **Phys. Chem, 2011, 13, 149–153**.

[16] *Macromolecular crowding: obvious but underappreciated.* R. J. Ellis. **TRENDS in Biochemical Sciences, Vol. 26, No. 10, October 2001**.

[17] *Photothermal Absorption Correlation Spectroscopy.* V. Octeau, L. Cognet, L. Duchesne, D. Lasne, N. Schaeffer, D. G. Fernig and B. Lounis. **ACSNano, Vol. 3, No. 2, 345–350, 2009**.

[18] *PDMS microfludic device for optical detection of protein immunoassay using gold nanoparticles.* C. Luo, Q. Fu,. H. Li, L. Xu, M. Sun, Q. Ouyang, Y. Chenb and H. Ji. **Lab Chip, 2005, 5, 726–729**.

Appendix A

Modelling of NP diffusion

Here we report the MATLAB code for calculating the diffusion coefficients as shown in fig. 3.1. From the same algorythm, with few changes, one can also plot the relative diffusion shift as in fig. 3.2.

```
clc
hold on

%% Input Data

NP_Diameter=linspace(10,100,20); % Nanoparticle diameter (nm)
Probe_Mass=54; % Mass of coating protein (kDa)
Target_Mass=25; % Mass of target Ab (kDa)
T=25; % Temperature of the medium

%% Start Computation
T=T+273.15; % Temperature in K

NP_Radius=NP_Diameter/2;

NP_Surface=4*pi*NP_Radius.^2;
NP_Volume=4/3*pi*NP_Radius.^3;

for Model=1:2
    switch Model

        case 1
            %% Case protein=polymer: Gyradius=7.257+0.395*N^3/5, N=#_aminoacids
            Model_Type='Protein=Polymer';
            Probe_AA=Probe_Mass/0.11;
            Probe_Radius=7.257+0.395*Probe_AA^(3/5);

            Target_AA=Target_Mass/(0.11);
            Target_Radius=7.257+0.395*Target_AA^(3/5);

        case 2
            %% Case protein=rigid sphere: Density=1.35 g/cm^3
            Model_Type='Protein=Rigid Sphere';
            Protein_Density=1.35/1.66*10; % Density (kDa/nm^3)

            Probe_Volume=Probe_Mass/Protein_Density;
            Probe_Radius=(Probe_Volume*3/4/pi)^(1/3);

            Target_Volume=Target_Mass/Protein_Density;
            Target_Radius=(Target_Volume*3/4/pi)^(1/3);

        otherwise
            disp('Model does not exist')

    end
```

```
    %% Diffusion Coefficient
    D0=1.38/10^23*T./(6*pi/10^3*NP_Radius/10^9); % D in SI unit

    NP_Probe_Radius=NP_Radius+2*Probe_Radius;
    D1=1.38/10^23*T./(6*pi/10^3*NP_Probe_Radius/10^9); % D in SI unit

    NP_Probe_Target_Radius=NP_Radius+2*Probe_Radius+2*Target_Radius;
    D2=1.38/10^23*T./(6*pi/10^3*NP_Probe_Target_Radius/10^9); % D in SI unit

    Delta_D=D1-D2;
    Rel_shift=Delta_D./D1;

    plot(NP_Diameter,D0,'-ok','MarkerSize',8);
    if Model==1,
        plot(NP_Diameter,D1,'-*r','MarkerSize',8);
        plot(NP_Diameter,D2,'-sr','MarkerSize',8);
    else
        plot(NP_Diameter,D1,'-+b','MarkerSize',8);
        plot(NP_Diameter,D2,'-xb','MarkerSize',8);
    end
    xlabel('NP Diameter (nm)');
    ylabel('Diffusion coefficient (m^2/s)');
end
```

Appendix B

FCS additional graphs

Fig. B.1 shows the time-trace and the autocorrelation curve of a FCS measurement of PBS pH7.4. One can easily see the artifact in the autocorrelation curve below 10 ms: for this reason we always fitted above this value.

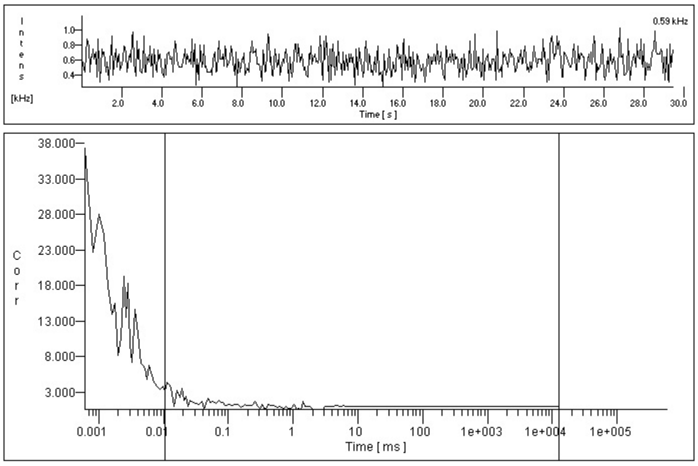

Figure B.1: **FCS PBS pH7.4.** Top, time-trace of PBS fluorescence (representing the background noise); bottom, autocorrelation curve.

Fig. B.2 shows the time-trace and the autocorrelation curve of a FCS measurement of 100% glycerol. The time-trace clearly shows the slightly larger fluorescence with respect to background noise.

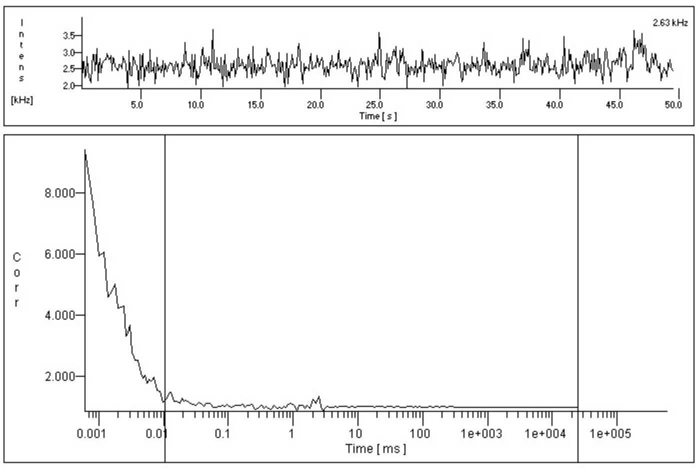

Figure B.2: **FCS 100% Glycerol.** Top, time-trace of glycerol fluorescence; bottom, autocorrelation curve.